Program (Grant DMR 8314193), and the U.S. Army Research Office (Contracts DAAG2985K0067 and DAAG2984G0080). B.C. thanks W. Buck for providing the PETFE polymers.

Registry No. (TFE)(E) (copolymer), 25038-71-5.

References and Notes

(1) Chu, B.; Ying, Q.; Wu, C.; Ford, J. R.; Dhadwal, H. S.; Qian, R.; Bao, J.; Zhang, J.; Xi, C. *Polym. Commun.* **1984**, *25*, 211.
(2) Ying, Q.; Chu, B. *Makromol. Chem., Rapid Commun.* **1984**, *5*, 785.
(3) Chu, B.; Wu, C.; Ford, J. R. *J. Colloid Interface Sci.* **1985**, *105*, 473.
(4) Ying, Q.; Chu, B.; Qian, R.; Bao, J.; Zhang, J.; Xu, C. *Polymer* **1985**, *26*, 1401.
(5) Chu, B.; Ying, Q.; Wu, C.; Ford, J. R.; Dhadwal, H. D. *Polymer* **1985**, *26*, 1408.
(6) Pope, J. W.; Chu, B. *Macromolecules* **1984**, *17*, 2633.
(7) Chu, B.; Onclin, M.; Ford, J. R. *J. Phys. Chem.* **1984**, *88*, 6566.
(8) For example, see: Chu, B.; Fytas, G.; Zalczer, G.; Lee, D. C.; Hagnauer, G. L. "Application of Light Scattering Spectroscopy to Polymerization Processes", invited presentation at the Symposium on Applications of Spectroscopy to Problems in Polymer Engineering and Science, 90th National Meeting of the American Institute of Chemical Engineers, Houston, TX, 1981.
(9) Chu, B.; Wu, C. *Macromolecules* **1986**, *19*, 1285.
(10) Adam, M.; Delsanti, M. *Macromolecules* **1977**, *10*, 1229.
(11) Miyaki, Y.; Einaga, Y.; Fujita, H. *Macromolecules* **1978**, *11*, 1180.
(12) Chu, B.; Lee, D.-C. *Macromolecules* **1984**, *17*, 926.
(13) English, A. D.; Garza, O. T. *Macromolecules* **1978**, *12*, 351.
(14) Modena, M.; Garbuglio, C.; Ragazzini, M. *J. Polym. Sci., Part B* **1972**, *10*, 153.
(15) Clark, D. T.; Feast, W. J.; Ritchie, I.; Musgrave, W. K. R. *J. Polym. Sci.* **1974**, *12*, 1049.

Light Scattering Characterization of an Alternating Copolymer of Ethylene and Tetrafluoroethylene. 2. Molecular Weight Distributions

Chi Wu,[†] Warren Buck,[‡] and Benjamin Chu*[†§]

Chemistry Department, State University of New York at Stony Brook, Long Island, New York 11794, Polymer Products Department, Experimental Station, E. I. du Pont de Nemours and Co., Inc., Wilmington, Delaware 19898, and Department of Materials Science and Engineering, State University of New York at Stony Brook, Long Island, New York 11794. *Received April 17, 1986*

ABSTRACT: By combining static and dynamic properties (M_w, A_2, k_d, R_g, and $D_0°$) of an alternating copolymer of ethylene and tetrafluoroethylene, $-(CF_2CF_2CH_2CH_2)_x-$, in diisobutyl adipate at 240 °C with a detailed analysis of the intensity–intensity time correlation function, we have been able to determine, for the first time, the molecular weight distribution (MWD) of an alternating copolymer of ethylene and tetrafluoroethylene (PETFE). A variety of Laplace inversion techniques, including multiexponential singular value decomposition (MSVD), a method of regularization (RILIE), and CONTIN, was used to obtain an estimate of the normalized characteristic line-width distribution function $G(\Gamma)$. The nonintrusive laser light scattering technique permits us to determine the molecular weight as well as the MWD of PETFE based on sound physical principles. Furthermore, in view of the simple $\Gamma = DK^2$ (with Γ, D, and K being the characteristic line width, the translational diffusion coefficient, and the magnitude of the momentum transfer vector, respectively) dependence and the second virial coefficient of diffusion, $k_d \sim 0$, the Laplace inversion used in the data analysis can be greatly simplified for determination of molecular weight and polydispersity of PETFE in diisobutyl adipate at 240 °C.

I. Introduction

In the previous paper (1), we characterized the solution properties of an alternating copolymer of ethylene (E) and tetrafluoroethylene (TFE), $-(CF_2CF_2CH_2CH_2)_x-$, denoted PETFE, in diisobutyl adipate at 240 °C, using laser light scattering intensity and line-width measurements. From light scattering intensity measurements, we obtained $\langle R_g^2\rangle_z^{1/2} = 1.68 \times 10^{-1} M_w^{0.60}$, with the z-average root-mean-square radius of gyration R_g [$\equiv\langle R_g^2\rangle_z^{1/2}$] and the weight-average molecular weight M_w expressed in units of Å and daltons, respectively. In combination with light scattering line-width measurements, we obtained $D_0° = 3.35 \times 10^{-4} M_w^{-0.60}$, with the translational diffusion coefficient at infinite dilution expressed in units of $cm^2\ s^{-1}$. In the present paper, the main steps are to obtain estimates of the normalized characteristic line-width distribution function $G(\Gamma)$ from the measured intensity–intensity time correlation function and to transform $G(\Gamma)$ to the molecular weight distribution (MWD) by means of the experimentally determined scaling relation $D_0° = k_D M^{-0.60}$. The main obstacle in the procedure is related to the relatively new method of data analysis: Laplace inversion of the electric field time correlation function:

$$g^{(1)}(K,\tau) = \int_0^\infty G(K,\Gamma) e^{-\Gamma(K)\tau}\, d\Gamma \qquad (1)$$

Although Laplace inversion is a difficult ill-posed problem because of the bandwidth limitation of our instrument and the noise in $g^{(1)}(K,\tau)$, there exists a variety of approaches (in particular, the method of regularization) permitting us to obtain approximate forms of $G(\Gamma)$ based on sound mathematical principles. Furthermore, several algorithms have undergone extensive tests using simulated data as well as actual experiments and have been applied to a variety of studies.[1,2] In an earlier laser light scattering study on the MWD of linear polyethylene,[3] we used the approach first developed by McWhirter and Pike,[4,5] while

[†] Chemistry Department, State University of New York at Stony Brook.
[‡] Polymer Products Department, E. I. du Pont de Nemours and Co.
[§] Department of Materials Science and Engineering, State University of New York at Stony Brook.

0024-9297/87/2220-0098$01.50/0

in a recent MWD characterization of poly(1,4-phenyleneterephthalamide),[6] we used the multiexponential singular value decomposition (MSVD) technique[2] with discrete multiexponentials to approximate $G(\Gamma)$ and a method of regularization (regularized inversion of the Laplace integral equation, designated RILIE) whereby a linearized smoothing operator[2] was used. In the present article, we added a widely used CONTIN algorithm developed by Provencher[7] for comparison purposes. It should be noted that for unimodal characteristic line-width distributions of relatively narrow polydispersity ($\mu_2/\bar{\Gamma}^2 < 0.2$), the cumulants method[8] of data analysis is applicable and yields valuable information in terms of the average line width $\bar{\Gamma}$ [$=\int \Gamma G(\Gamma)\, d\Gamma$] and the variance $\mu_2/\bar{\Gamma}^2$ with $\mu_2 = \int(\Gamma - \bar{\Gamma})^2 G(\Gamma)\, d\Gamma$.

II. Laplace Transform

The MSVD technique,[1,2,6] the RILIE regularization method,[2,6] and Provencher's CONTIN program[1,7] have been described in detail elsewhere. We only outline the essential steps that are necessary in describing our data fitting results.

1. MSVD Technique. In the MSVD technique, we approximate $G(\Gamma)$ by a set of linearly or logarithmically spaced discrete single exponentials:

$$G(\Gamma) = \sum_j P_j \delta(\Gamma - \Gamma_j) \tag{2}$$

such that b_i [$\equiv g^{(1)}(\tau_i) = \int G(K,\Gamma) e^{-\Gamma(K)\tau_i}\, d\Gamma$] $= \sum_j P_j \exp(-\Gamma_j \tau_i)$, with P_j being the weighting factors of the δ functions. The linear least-squares minimization problem has the form $\mathbf{CP} \simeq \mathbf{b}$, with the symbol "$\simeq$" intended to imply solution of the overdetermined set of equations subject to minimization of the Euclidean norm of the residual vector $\|\mathbf{b} - \mathbf{CP}\|$ and the elements of $\mathbf{C}$ being $C_{ij} = e^{-\Gamma_j \tau_i}$. $\mathbf{P}$ and $\mathbf{b}$ are vectors and $\mathbf{C}$ is an $i \times j$ matrix. The MSVD technique yields a discrete distribution for $G(\Gamma)$ and is applicable for unimodal $G(\Gamma)$.

2. Regularization Method (RILIE). Our regularization method was a modified version of the one developed by Abbiss et al.[9] for laser Doppler velocimetry. The regularization method imposes stability on the solution by using reasonable constraints. It attempts to solve a related equation whose solution responds stably to perturbations in the data and yet is constrained to be close to the distribution $G(\Gamma)$. In the iterative scheme, the choice of the smoothing parameter (α) is crucial. α should be as close to zero as possible in order to allow the maximum amount of information to be retrieved from the data while still retaining the stability of the solution. Our regularization method yields a continuous distribution for $G(\Gamma)$.

III. Results and Discussion

By following experimental procedures for self-beating and base-line considerations,[6,10] we could obtain precise measurements of the intensity–intensity time correlation function $G^{(2)}(K,\tau)$:

$$G^{(2)}(K,\tau) = A(1 + b|g^{(1)}(K,\tau)|^2) \tag{3}$$

where the base line A agreed with the measured base line $\lim_{\tau\to\infty} G^{(2)}(K,\tau)$ to within about 0.1%. Figure 1a shows a typical experimental intensity–intensity photoelectron count autocorrelation function for PETFE in diisobutyl adipate measured at $\theta = 30°$ and 240 °C using a delay time increment $\Delta\tau$ of 22.5 μs. Relative deviation plots of the measured and the computed time correlation function using three different methods of Laplace inversion (MSVD, RILIE, and CONTIN) as well as the method of cumulants (second order) are shown in Figure 1b. In Figure 1b, we clearly see that there are different approaches to seeking approximate solutions to the Laplace inversion, even though all three algorithms essentially invoke the method of regularization. It should also be noted that, in an ill-posed problem, goodness of fit does not guarantee a correct solution to the inversion. The treatment of the ill-posed Laplace inversion problem was based on sound principles developed by mathematicians.[11] In photon correlation spectroscopy, the algorithms deal with practical applications of the method of regularization using different criteria. Each algorithm has a mathematically defined most probable solution to the Laplace inversion problem. However, there is always an element of uncertainty because we do not know precisely the signal-to-noise ratio of our measurements. This is not to say that we do not know our counting statistics (which we do). Rather, these are experimental noises due perhaps to dust particles, laser fluctuations, system noise, or trace amounts of stray light.

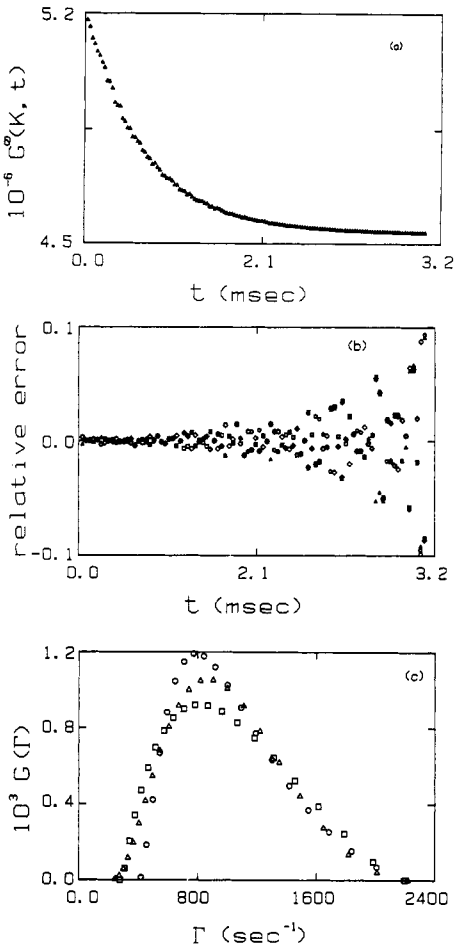

Figure 1. (a) A typical unnormalized intensity–intensity autocorrelation function for 4.03 mg mL^{-1} PETFE ($M_w = 5.4 \times 10^5$) in diisobutyl adipate measured at $\theta = 30°$ and 240 °C using a delay time increment $\Delta\tau$ of 22.5 μs. (b) Relative deviation plots of the measured and the computed time correlation function using different methods of Laplace inversion as well as the method of cumulants (second order). Relative deviation = $(b|g^{(1)}(t)|^2)_{measd} - (b|g^{(1)}(t)|^2)_{calcd}/(b|g^{(1)}(t)|^2)_{measd}$. (c) Normal characteristic line-width distribution for (a) using different methods of Laplace inversion. Results of computations are summarized in Table I. Numerical values of $G(\Gamma)$ using different methods of data analysis are listed in Table II. Filled triangles denote the experimentally measured intensity–intensity time correlation function $G^{(2)}(K,t)$. Hollow circles denote computed results based on MSVD. Hollow squares denote computed results based on our regularization method RILIE. Hollow triangles denote computed results based on CONTIN. Hollow diamonds denote computed results based on second-order cumulants expansion.

Table I
Experimental Results Based on Different Algorithms for PETFE I in Diisobutyl Adipate at 240 °C
(M_w = 5.4 × 10^5; θ = 30°; C = 4.03 mg mL^{-1})

	PETFE I[a]				PETFE II-I[b]
parameter	MSVD	RILIE	CONTIN	cumulants	(eq 6)
$\bar{\Gamma}$, s^{-1}	1.00 × 10^3	1.03 × 10^3	1.01 × 10^3	1.03 × 10^3	
$\mu_2/\bar{\Gamma}^2$	0.10	0.11	0.10	0.097	0.11
M_z:M_w:M_n	2.0:1.3:1	2.2:1.4:1	2.0:1.3:1		

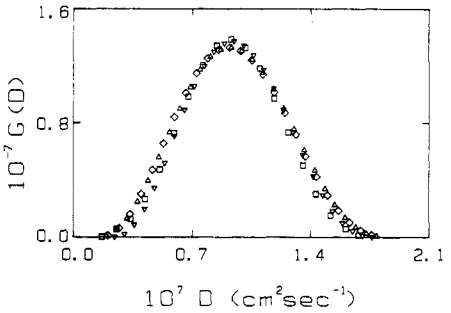

Figure 2. Plots of $G(D)$ vs. D (=Γ/K^2) for 3.50 mg mL^{-1} PETFE (M_w = 9.0 × 10^5) in diisobutyl adipate at 240 °C based on the CONTIN method of data analysis: (□) θ = 30°, $\bar{D}$ = 9.35 × 10^{-8} cm^2 s^{-1}, $\mu_2/\bar{\Gamma}^2$ = 0.10; (◇) θ = 40°, $\bar{D}$ = 9.12 × 10^{-8} cm^2 s^{-1}, μ_2/Γ^2 = 0.096; (△) θ = 50°, $\bar{D}$ = 9.25 × 10^{-8} cm^2 s^{-1}, $\mu_2/\bar{\Gamma}^2$ = 0.10; (▽) θ = 60°, $\bar{D}$ = 9.24 × 10^{-8} cm^2 s^{-1}, $\mu_2/\bar{\Gamma}^2$ = 0.09. Overall $\bar{D}$ = 9.24 × 10^{-8} cm^2 s^{-1}.

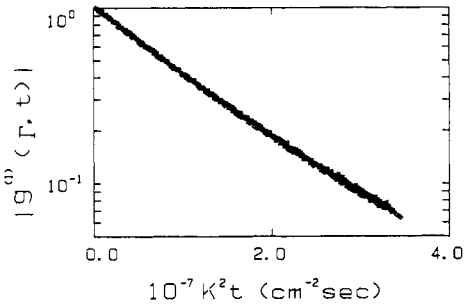

Figure 3. Scaling of $|g^{(1)}(\Gamma,t)|$ at different scattering angles by K^2 at constant concentration C = 3.50 mg mL^{-1} for PETFE (M_w = 9.0 × 10^5) in diisobutyl adipate at 240 °C. Same symbols as in Figure 2.

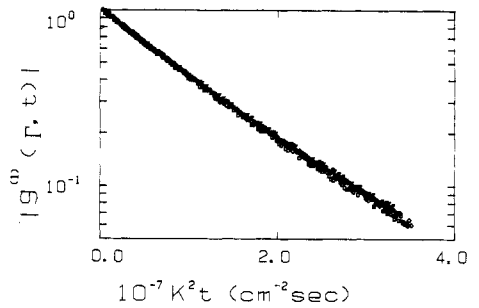

Figure 4. Scaling of $|g^{(1)}(\Gamma,t)|$ due to concentration effect at constant scattering angle (θ = 30°) for PETE (M_w = 9.0 × 10^5) in diisobutyl adipate at 240 °C. Analysis by second-order cumulants method. (◇) C = 1.22 mg mL^{-1}, $\bar{D}$ = 9.15 × 10^{-8} cm^2 s^{-1}, $\mu_2/\bar{\Gamma}^2$ = 0.09; (□) C = 2.30 mg mL^{-1}, $\bar{D}$ = 9.31 × 10^{-8} cm^2 s^{-1} $\mu_2/\bar{\Gamma}^2$ = 0.09; (▽) C = 2.94 mg mL^{-1}, $\bar{D}$ = 9.00 × 10^{-8} cm^2 s^{-1} $\mu_2/\bar{\Gamma}^2$ = 0.11; (○) C = 3.50 mg mL^{-1}, $\bar{D}$ = 9.35 × 10^{-8} cm^2 s^{-1} $\mu_2/\bar{\Gamma}^2$ = 0.10; (△) C = 4.25 mg mL^{-1}, $\bar{D}$ = 9.06 × 10^{-8} cm^2 s^{-1} $\mu_2/\bar{\Gamma}^2$ = 0.095. Overall $\bar{D}$ ≃ 9.15 × 10^{-8} cm^2 s^{-1}; overall $\mu_2/\bar{\Gamma}^2$ ≃ 0.10.

Furthermore, optimization of the finite bandwidth range in the measured intensity–intensity time correlation in order to retrieve a maximum amount of information on $G(\Gamma)$ has not been worked out precisely. Thus, we have used simulated data and known polymer systems under comparable experimental conditions, counting rates, and statistics to test our algorithms for the Laplace inversion. The agreement, as shown in Figure 1c and Table I, confirms that our results are independent of the method of data analysis. Numerical results of the transform by MSVD, RILIE, and CONTIN for the experimental data shown in Figure 1a and plotted in Figure 1c are listed in Table II. For unimodal distributions within a reasonable range of polydispersity, we can measure the molecular weight to within a few percent, the width of MWD to perhaps ~10%, and the skewness to ~50%. It is also difficult to locate the upper and lower bounds of $G(\Gamma)$.[12] Similar critique could be directed to other analytical techniques involving inversion of ill-conditioned integral equations. Unfortunately, most such treatments of data analysis have not yet reached the sophistication of the regularization method. It should also be noted that discrete and continuous normalized characteristic line-width distributions based on MSVD and RILIE (or CONTIN) algorithms are not the same. In a discrete $G(\Gamma)$, we have eq 2. If Γ_j does not have equal spacing, P_j has to be rescaled. In other words, $G(\Gamma) \neq G(\ln \Gamma)$.

From $G(\Gamma)$ and our knowledge on the simple K^2 dependence of $\bar{\Gamma}$ as well as a lack of the concentration dependence of the translational diffusion coefficient D°, i.e., the second virial diffusion coefficient $k_d \sim 0$, in which $D^\circ = \lim_{K\to 0} \bar{\Gamma}/K^2 = D_0^\circ(1 + k_dC)$, we can make a relatively simple conversion from $G(\Gamma)$ to $G(D_0^\circ)$. Figure 2 shows plots of $G(D)$ vs. D for 3.50 mg mL^{-1} PETFE (M_w = 9.0 × 10^5) in diisobutyl adipate at 240 °C and θ = 30° (hollow squares), 40° (hollow diamonds), 50° (hollow triangles), and 60° (hollow inverted triangles) based on the CONTIN method of data analysis. In the comparison, we not only have taken $D = \Gamma/K^2$ but have essentially assumed that $R_{vv}(K)$ was relatively constant over the θ = 30–60° angular range. In practice, we prefer to use the lower angle ($\theta \sim$ 30°) $G^{(2)}(K,\tau)$ as a basis for the transformation of variables in order to obtain the molecular weight distribution. Nevertheless, this approximation is acceptable for PETFE in diisobutyl adipate at 240 °C so long as its molecular weight range remains within 10^6 daltons or $KR_g \ll 1$. Figure 3 shows the scaling of $|g^{(1)}(\Gamma(K),t)|$ at different scattering angles by K^2, indicating the lack of interference effect at constant concentration (C = 3.50 mg mL^{-1}) for PETFE (M_w = 9.0 × 10^5) in diisobutyl adipate at 240 °C. Similarly, Figure 4 shows the scaling of $|g^{(1)}(\Gamma(K),\tau)|$ due to concentration effect at a constant angle (θ = 30°) for PETFE (M_w = 9.0 × 10^5) in diisobutyl adipate at 240 °C. The corresponding plots of $G(\Gamma)$ vs. Γ from the measured time correlation function based on the CONTIN method of data analysis are shown in Figure 5. The agreement in $\bar{D}$ (=$\bar{\Gamma}/K^2$) at θ = 30° over a range of concentrations as shown in the figure caption of Figure 5 confirms our earlier finding that $k_d \sim 0$ in $D^\circ = D_0^\circ(1 + k_dC)$, with $D^\circ = \lim_{K\to 0} \bar{\Gamma}/K^2 \simeq \bar{\Gamma}(\theta{=}30°)/K^2$. It should be noted that corrections to concentration and interference effects become appreciable whenever $k_dC \sim 1$ and $kR_g \gtrsim 1$, and such have been discussed elsewhere.[6] In the present case, at θ = 30°, $KR_g \sim 2 \times 10^{-2} < 1$ and $k_dC \ll 1$. Thus, within the precision of our analysis, we can simplify the transform by ignoring both extrapolations (to infinite dilution and zero scattering angle).

Table II
Data for $G(\Gamma)$ vs. Γ Using Different Methods of Data Analysis for PETFE I ($M_w = 5.4 \times 10^5$; $C = 4.03 \times 10^{-3}$ g mL^{-1}; $\theta = 30°$)

RILIE		CONTIN		MSVD	
Γ, s^{-1}	$G(\Gamma)$	Γ, s^{-1}	$G(\Gamma)$	Γ, s^{-1}	$G(\Gamma)$
2.79×10^2	0	2.47×10^2	4.75×10^{-6}	4.20×10^2	1.35×10^{-5}
3.09×10^2	6.06×10^{-5}	3.73×10^2	2.23×10^{-5}	4.58×10^2	1.84×10^{-4}
3.43×10^2	2.04×10^{-4}	3.02×10^2	5.82×10^{-5}	5.00×10^2	4.22×10^4
3.80×10^2	3.42×10^{-4}	3.33×10^2	1.16×10^{-4}	5.45×10^2	6.67×10^{-4}
4.20×10^2	4.72×10^{-4}	3.68×10^2	1.96×10^{-4}	5.95×10^2	8.82×10^{-4}
4.67×10^2	5.91×10^{-4}	4.07×10^2	2.98×10^{-4}	6.49×10^2	1.04×10^{-3}
5.18×10^2	6.96×10^{-4}	4.50×10^2	4.16×10^{-4}	7.08×10^2	1.15×10^{-3}
5.74×10^2	7.85×10^{-4}	4.97×10^2	5.46×10^{-4}	7.71×10^2	1.19×10^{-3}
6.37×10^2	8.53×10^{-4}	5.49×10^2	6.80×10^{-4}	8.42×10^2	1.17×10^{-3}
7.06×10^2	8.99×10^{-4}	6.07×10^2	8.07×10^{-4}	9.18×10^2	1.12×10^{-3}
7.83×10^2	9.21×10^{-4}	6.71×10^2	9.16×10^{-4}	1.00×10^3	1.02×10^{-3}
8.68×10^2	9.16×10^{-4}	7.41×10^2	1.00×10^{-3}	1.09×10^3	9.06×10^{-4}
9.63×10^2	8.86×10^{-4}	8.19×10^2	1.05×10^{-3}	1.19×10^3	7.72×10^{-4}
1.07×10^3	8.30×10^{-4}	9.05×10^2	1.05×10^{-3}	1.30×10^3	6.34×10^{-4}
1.18×10^3	7.48×10^{-4}	1.00×10^3	1.01×10^{-3}	1.42×10^3	4.97×10^{-4}
1.31×10^3	6.45×10^{-4}	1.11×10^3	9.15×10^{-4}	1.55×10^3	3.69×10^{-4}
1.46×10^3	5.24×10^{-4}	1.22×10^3	7.82×10^{-4}	1.69×10^3	2.53×10^{-4}
1.61×10^3	3.88×10^{-4}	1.35×10^3	6.19×10^{-4}	1.84×10^3	1.53×10^{-4}
1.79×10^3	2.44×10^{-4}	1.49×10^3	4.43×10^{-4}	2.01×10^3	6.92×10^{-5}
1.98×10^3	9.61×10^{-5}	1.65×10^3	2.74×10^{-4}	2.19×10^3	1.73×10^{-6}
2.20×10^3	0	1.82×10^3	1.34×10^{-4}		
		2.01×10^3	4.14×10^{-4}		
		2.22×10^3	0		

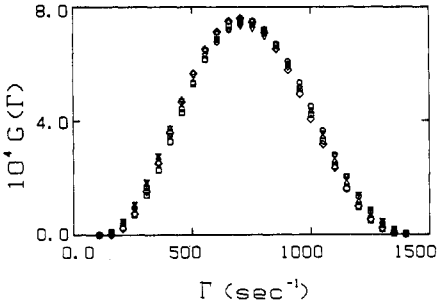

Figure 5. Plots of $G(\Gamma)$ vs. Γ for the same $|g^{(1)}(\Gamma,t)|$ as in Figure 4 at different concentrations based on the CONTIN method. Same symbols as in Figure 4. PETFE ($M_w = 9.0 \times 10^5$) g in diisobutyl adipate at 240 °C at $\theta = 30°$. (◇) $C = 1.22$ mg mL^{-1}, $\bar{D} = 9.35$ cm^2 s^{-1}, $\mu_2/\bar{\Gamma}^2 = 0.10$; (□) $C = 2.30$ mg mL^{-1}, $\bar{D} = 9.13$ cm^2 s^{-1}, $\mu_2/\bar{\Gamma}^2 = 0.10$; (▽ $C = 2.94$ mg mL^{-1}, $\bar{D} = 9.11$ cm^2 s^{-1}, $\mu_2/\bar{\Gamma}^2 = 0.11$; (○) $C = 3.50$ mg mL^{-1}, $\bar{D} = 9.28$ cm^2 s^{-1}, $\mu_2/\bar{\Gamma}^2 = 0.10$; (△) $C = 4.25$ mg mL^{-1}, $\bar{D} = 8.96$ cm^2 s^{-1}, $\mu_2/\bar{\Gamma}^2 = 0.10$.

Having computed $G(D_0°)$ [$\simeq G(D)$, as shown in Figure 2], we now make use of the empirical relation for the translational diffusion coefficient $D_{0,j}°$ (in cm^2 s^{-1}) = $3.35 \times 10^{-4} M_j^{-0.60}$ for each fraction of PETFE having molecular weight M_j expressed in daltons. At each scattering angle, the excess Rayleigh ratio has the form

$$R_{vv}(K) \sim \int F_n(M) M^2 P(M,K)\, dM \qquad (4)$$

where $P(M,K)$ is the particle scattering factor and $F_n(M)$ is the normalized number distribution for PETFE. The "$\sim$" sign denotes that we are not concerned with the proportionality constant. At small enough scattering angles, $P_j \sim F_n(M_j) M_j^2 P(M_j) \simeq F_n(M_j) M_j^2$ as $P(M_j) \simeq 1$. The first-order term for $P(M_j)$ has the form $P(M_j) \simeq 1 - R_g^2(M_j) K^2/3$. Thus, we can correct for the interference effect in the molecular weight distribution since we have the empirical scaling relation between the radius of gyration and the molecular weight: $R_{g,j}$ (in Å) = $1.68 \times 10^{-1} M_j^{0.60}$, with M_j expressed in daltons.

Figure 6 shows a typical normalized weight distribution ($f_w \sim F_n M$) of PETFE ($M_w = 5.4 \times 10^5$) using three different algorithms of Laplace inversion (MSVD, RILIE, and CONTIN) all based on the regularization method. The results of our analysis for the three PETFE polymer samples are summarized in Table III. The three molecular weight distributions for PETFE I as listed in Table III show similar M_z:M_w:M_n as well as the values for the M_w ($\approx (5.3 \pm 0.1) \times 10^5$), which compares favorably with the M_w value (5.4×10^5) determined by absolute light scattering intensity measurements. We are, of course, aware of the fact that the empirical relation for $D_0° = k_D M^{-\alpha_D}$

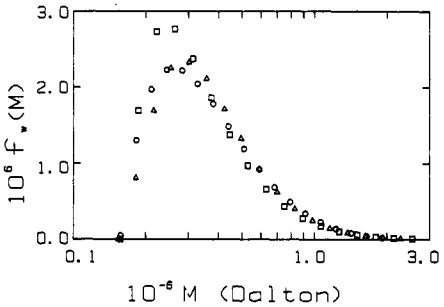

Figure 6. Molecular weight distribution of PETFE I using three different methods (MSVD, RILIE, and CONTIN). Hollow triangles denote CONTIN, hollow squares denote RILIE, and hollow circles denote MSVD. The results are summarized in Table III under PETFE I.

Table III
Molecular Parameters of PETFE Polymer Samples in Diisobutyl Adipate at 240 °C ($D_0° = 3.35 \times 10^{-4} M^{-0.60}$; $k_d = 0$)

parameter	MSVD	RILIE	CONTIN
PETFE I			
$M_w = 5.4 \times 10^5$, $R_g = 454$ Å, $A_2 = 1.97 \times 10^{-4}$ mol mL g^{-2}			
M_w	5.3×10^5	5.2×10^5	5.4×10^5
M_n	4.0×10^5	3.7×10^5	4.0×10^5
M_z:M_w:N_n	2.0:1.3:1	2.2:1.4:1	2.0:1.3:1
PETFE II			
$M_w = 9.0 \times 10^5$, $R_g = 619$ Å, $A_2 = 1.14 \times 10^{-4}$ mol mL g^{-2}			
M_w	8.9×10^5	8.9×10^5	9.0×10^5
M_n	6.4×10^5	6.8×10^5	7.0×10^5
M_z:M_w:M_n	2.1:1.4:1	2.3:1.3:1	2.0:1.3:1
PETFE III			
$M_w = 1.16 \times 10^6$, $R_g = 721$ Å, $A_2 = 1.02 \times 10^{-4}$ mol mL g^{-2}			
M_w	1.14×10^6	1.15×10^6	1.18×10^6
M_n	8.1×10^5	8.8×10^5	8.4×10^5
M_z:M_w:M_n	2.0:1.4:1	2.2:1.3:1	2.1:1.4:1

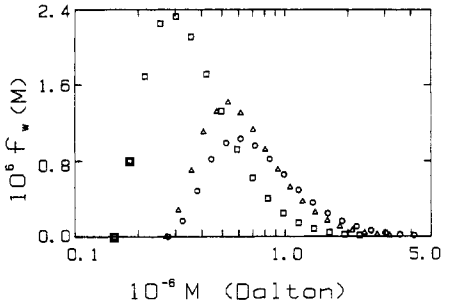

Figure 7. Molecular weight distributions of PETFE based on the CONTIN method of data analysis. Characteristics of the MWD are listed in Table III.

Table IV
Scaling Relations[a] and Molecular Weight Ratios of Curves Shown in Figure 8 (θ = 30°; C = 4.03 mg mL^{-1}; M_w = 5.4 × 10^5)

symbol	$D_0°$ (cm^2 s^{-1}) = $k_D M^{-\alpha_D}$ (g mol^{-1})	$M_n \times 10^{-5}$	M_z:M_w:M_n
□	$D_0° = 3.75 \times 10^{-4} M^{-0.60}$	3.9	2.2:1.4:1
○	$D_0° = 2.70 \times 10^{-4} M^{-0.575}$	3.8	2.3:1.4:1
△	$D_0° = 1.96 \times 10^{-4} M^{-0.55}$	3.7	2.4:1.4:1

[a] M_w was set at 5.4 × 10^5 based on the static light scattering experiment.

was calibrated by means of absolute light scattering measurements. The main point here is to illustrate that our analysis is self-consistent. The laser light scattering (LLS) approach for the determination of MWD has its own internal absolute calibration. Figure 7 shows the molecular weight distributions of the three PETFE polymer samples that we have examined. It is amazing to note that $M_w/M_n \sim 1.3$ for all three PETFE polymer samples. Such narrow MWD's cannot be attributed to known experimental errors. If there were internal motions, the additional high-frequency components would broaden the characteristic line-width distribution $G(\Gamma)$. Similarly, the introduction of a small amount of stray light or dust would broaden the high- or low-frequency limits of $G(\Gamma)$. With $M_w/M_n \sim 1.3$, LLS can determine the variance $(\mu_2/\bar{\Gamma}^2)$ by any of the standard methods of data analysis, including the cumulants method. In our analysis, we have assumed PETFE to be highly alternating[15] and the E/TFE composition to be essentially independent of molecular weight.

In paper 1, we have noted that the diffusion/molecular weight scaling exponent α_D has an estimated value of 0.6, corresponding to the maximum limit for a polymer coil in a good solvent. As we were able to cover a molecular weight range by only a factor of 2 and the magnitudes of the second virial coefficients, k_d and A_2, were relatively small, we should qualify the value of 6 by denoting the effect of its magnitude on the MWD. Figure 8 shows plots of MWD for α_D values of 0.60 (□), 0.575 (○), and 0.55 (△) with the scaling relations and resultant molecular weight ratios listed in Table IV. We note that the exact value of α_D is not very important in our determination of MWD.

Finally, it is feasible to utilize the difference correlation functions for on-line monitoring of molecular weight and polydispersity changes. Figure 9 shows plots of log $|g^{(1)}(\Gamma,\tau)|$ (left-side y axis) as a function of K^2t for PETFE I, II, and III. If we take PETFE II as our reference standard, we can observe the changes in molecular weight purely from the slopes of PETFE II-I and PETFE III-II using any combination of scattering angle and concentration since $KR_g \lesssim 1$ and $k_dC \ll 1$. In the cumulants expansion

$$\ln |g^{(1)}(t)| = -\bar{\Gamma}t + (1/2)\mu_2 t^2 + \ldots \quad (5)$$

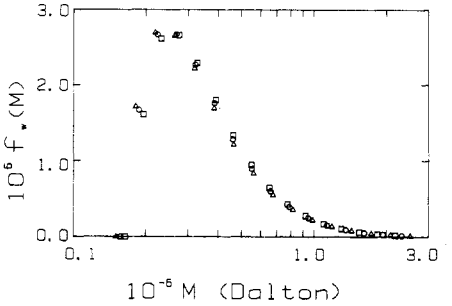

Figure 8. Molecular weight distributions of PETFE based on the CONTIN method of data analysis and different values of α_D but constant M_w with the scaling relations and the resultant molecular weight ratios listed in Table IV. Data from θ = 30°, C = 4.03 mg mL^{-1}, 240 °C, and M_w = 5.4 × 10^5 PETFE in diisobutyl adipate.

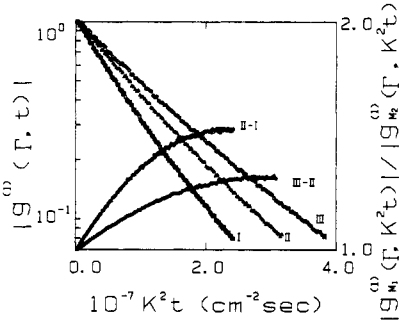

Figure 9. Scaling of $|g^{(1)}(\Gamma,t)|$ at different molecular weights. θ = 30°. Note: concentration has negligible effects. (□) PETFE I, M_w = 5.40 × 10^5, C = 4.03 × 10^{-3} mg mL^{-1}; (△) PETFE II, M_w = 9.00 × 10^5, C = 3.50 × 10^{-3} mg mL^{-1}; (○) PETFE III, M_w = 1.16 × 10^6, C = 4.28 × 10^{-3} mg mL^{-1}. Y = log $|g^{(1)}(\Gamma,t)|$ − log $|g^{(1)}(\Gamma,t)|$. PETFE II-I, slope = 1.27 × 10^{-8} cm^2 s^{-1} (M_w(PETFE I) from Figure 8 = 5.62 × 10^5, M_w(PETFE I) from intensity = 5.40 × 10^5, M_w(PETFE I) from line width = 5.3 × 10^5); PETFE III-II, slope 4.97 × 10^{-9} cm^2 s^{-1} (M_w(PETFE III) from Figure 8 = 1.13 × 10^6, M_w(PETFE III) from intensity = 1.16 × 10^6, M_w(PETFE III) from line width = 1.18 × 10^6).

and the difference term for the two molecular weights can be represented by

$$\log |g_{M_1}^{(1)}(\Gamma,K^2t)| - \log |g_{M_2}^{(1)}(\Gamma,K^2t)| \simeq -\frac{k_D}{2.303}[M_1^{-0.6} - M_2^{-0.6}]K^2t + \frac{1}{4.606K^4}(\mu_{2,M_1} - \mu_{2,M_2})K^4t^2 \quad (6)$$

In eq 6, the first term on the right-hand side corresponds to the initial slope in a plot of log $|g_{M_1}^{(1)}(\Gamma,K^2t)|$ − log $|g_{M_2}^{(1)}(\Gamma,K^2t)|$ vs. K^2t as shown in Figure 9, with $Y \equiv$ log $|g_{M_1}^{(1)}(\Gamma,K^2t)|$ − log $|g_{M_2}^{(1)}(\Gamma,K^2t)|$ being the right-side y axis. By least-squares fitting of the difference curves, we determined the molecular weights of PETFE I and III to be 5.62 × 10^5 and 1.13 × 10^6 using eq 6 and M_w(PETFE II) = 9.00 × 10^5. It is interesting to note that the computed $\mu_2/\bar{\Gamma}^2$ values are in agreement with the detailed computations; e.g., see Table I for results of PETFE I, confirming that the polydispersity index M_w/M_n (~1.3) has remained relatively unchanged. Thus, with a reference curve as our standard, we can determine the molecular weight and the polydispersity index (M_w/M_n) for PETFE in diisobutyl adipate at 240 °C without the use of Laplace inversion. The results can be computed easily by a hand-held calculator or estimated by eye inspection!

After characterization of PETFE, we realize that the polymer coil behaves fairly normally. Figure 10 shows a log–log plot of η_{melt} vs. M_w. We obtained

$$\eta_{melt}\ (\text{Poise}) = 1.88 \times 10^{-20} M_w^{3.42} \quad (7)$$

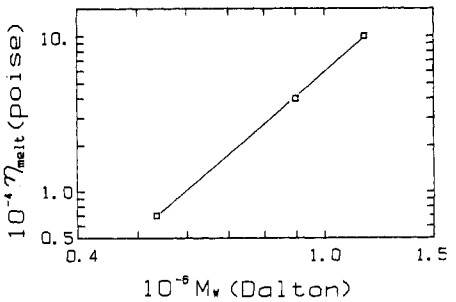

Figure 10. log–log plot of η_{melt} vs. M_w at 297 °C. $\eta_{melt} = 1.88 \times 10^{-20} M_w^{3.42}$, with η_{melt} and M_w expressed in units of poise and daltons, respectively.

confirming the experimental viscosity exponent of 3.4. With eq 7, it is now possible to determine the molecular weight of PETFE in the melt state by means of high-temperature rheometry so long as the molecular weight of PETFE remains sufficiently high for the melt viscosity exponent value of 3.4 to hold.

IV. Conclusions

Laser light scattering, including measurements of the angular distribution of the absolute scattered intensity and of the time correlation function together with correlation function profile analysis, has been developed into a powerful analytical tool for polymer characterizations. We have succeeded in determining the molecular weight and its distribution of polymers, which are very difficult to characterize by standard analytical techniques. Aside from polyethylene in trichlorobenzene, poly(1,4-phenyleneterephthalamide) in concentrated sulfuric acid, and poly(ethylene terephthalate) in hexafluoro-2-propanol, we have now characterized an alternating copolymer of ethylene and tetrafluoroethylene. In each case, the problem has often been much more than just searching for an appropriate solvent for the polymer. For the PETFE characterization, we had to develop a new apparatus for polymer dissolution and solution clarification at high temperatures, a new light scattering spectrometer, and improved methods of data analysis. The technology has now been developed and demonstrated under the most stringent conditions. By coupling with other separation techniques, the LLS detection technique using a flow cell[14] should have great potential as an analytical tool for polymer and colloidal particle characterizations.

Acknowledgment. We gratefully acknowledge support of this research by the National Science Foundation, Polymers Program (Grant DMR 8314193), the Petroleum Research Fund, administered by the American Chemical Society, and the U.S. Army Research Office (Contracts DAAG2985K0067 and DAAG2984G0080).

Registry No. (TFE)(E) (copolymer), 25038-71-5.

References and Notes

(1) See: Schulz-DuBois, E. O., Ed. *Proceedings of the 5th International Conference on Photon Correlation Techniques in Fluid Mechanics* (Springer Series in Optical Sciences); Springer-Verlag: New York, 1983.
(2) Chu, B.; Ford, J. R.; Dhadwal, H. S. In *Methods Enzymol.* **1983**, *117*, 256–297.
(3) Pope, J. W.; Chu, B. *Macromolecules* **1984**, *17*, 2633.
(4) McWhirter, J. G.; Pike, E. R. *J. Phys. A* **1978**, *11*, 1729.
(5) Ostrowski, N.; Sornette, D.; Parker, P.; Pike, E. R. *Opt. Acta* **1981**, *28*, 1059.
(6) Chu, B.; Ying, Q.-C.; Wu, C.; Ford, J. R.; Dhadwal, H. S. *Polymer* **1985**, *26*, 1408.
(7) Provencher, S. W. *Biophys. J.* **1976**, *16*, 27; *J. Chem. Phys.* **1976**, *64*, 2772; *Makromol. Chem.* **1979**, *180*, 201.
(8) Koppel, D. E. *J. Chem. Phys.* **1972**, *57*, 4814.
(9) Abbiss, J. B.; Demol, C.; Dhadwal, H. D. *Opt. Acta* **1983**, *30*, 107.
(10) Chu, B. In *The Application of Laser Light Scattering to the Study of Biological Motion*; Earnshaw, J. C., Steer, M. W., Eds.; Plenum: New York, 1983; pp 53–76.
(11) See for example: Miller, K. *SIAM J. Math. Anal.* **1970**, *1*, 52. Tikhonov, A. N.; Arsenin, V. Y. *Solutions of Ill-Posed Problems*, V. H. Winston: Washington, D.C., 1977.
(12) Chu, B. *Polym. J. (Tokyo)* **1985**, *17*, 225.
(13) Chu, B.; Wu, C.; Ford, J. R. *J. Colloid Interface Sci.* **1985**, *105*, 473.
(14) Chu, B.; Park, I. H.; Ford, J. R. *Polym. Prepr. (Am. Chem. Soc., Div. Polym. Chem.)* **1983**, *24*, 237.
(15) English, A. D.; Garza, O. T. *Macromolecules* **1979**, *12*, 351.

Dynamics of a Flexible Polymer Chain in Steady Shear Flow: The Rouse Model

J. A. Y. Johnson*

Hasbrouck Laboratory, Department of Physics and Astronomy, University of Massachusetts, Amherst, Massachusetts 01003. *Received June 9, 1986*

ABSTRACT: The Rouse model of a flexible polymer in dilute solution is studied. A complete description of the dynamics of a Hookean dumbbell in shear flow is developed from the Bose operator representation of the Smoluchowski equation. The relaxation of fluctuations from the nonequilibrium steady state is examined, and dynamic correlation functions are determined exactly. The results are used to study the dynamics of the Rouse chain in shear flow.

I. Introduction

The theoretical study of dilute polymer solutions has contributed considerably to the understanding of polymer flow properties (see, e.g., ref 1–4). In dilute solutions, with which this paper is concerned, interchain interactions are negligible, and, therefore, each chain contributes independently to the flow properties and can be treated separately. The bead–spring models, which represent a polymer molecule by a chain of beads connected by springs (see Figure 1), have had notable success in describing dilute solutions of flexible polymers.[2] In these models, the springs represent nearest-neighbor interactions between beads, which represent segments of the polymer; non-nearest-neighbor interactions can also be included. The beads also

* Present address: Department of Polymer Science and Engineering, University of Massachusetts, Amherst, MA 01003.

0024-9297/87/2220-0103$01.50/0